A New Algorithm to Eliminate GPS Carrier-Phase Time Transfer Boundary Discontinuity

Jian Yao and Judah Levine

Time and Frequency Division and JILA, National Institute of Standards and Technology and University of Colorado, Boulder, Colorado 80305, USA

E-mail*: jian.yao@colorado.edu*

BIOGRAPHY

Jian Yao was born in Nancheng, Jiangxi Province, China, in 1988. He received bachelor of science degree in physics from Nanjing University, China, in 2009, and master of science degree in physics from University of Colorado at Boulder in 2012. He is currently a graduate student at the University of Colorado at Boulder and National Institute of Standards and Technology (NIST), where he performs studies in GPS carrier-phase time and frequency transfer under the supervision of Dr. Judah Levine.

Judah Levine is a Fellow of the National Institute of Standards and Technology and is the leader of the Network Synchronization Project in the Time and Frequency Division, which is located in the NIST laboratories in Boulder, Colorado. Dr. Levine is responsible for the design and implementation of the time scales AT1 and UTC(NIST), which provide the reference signals for all of the NIST time and frequency services. In addition, he designed and built the servers that support the Automated Computer Time Service (ACTS) and the Internet Time Service, which provide time and frequency information to users in a number of different digital formats. The ACTS service is realized using a number of parallel computers that control a 12-line telephone rotary. The ACTS service receives about 4,000 requests per day. The Internet Time Service uses 24 computers which are located at several sites in the US. These computers receive about 6500 million (6.5 billion) requests per day for time stamps in 3 different standard formats. He received his Ph.D. in Physics from New York University in 1966. Dr. Levine is a member of the IEEE and a Fellow of the American Physical Society.

ABSTRACT

We report on a study of the Global Positioning System (GPS) carrier-phase (CP) time transfer boundary discontinuity by the use of the precise point positioning (PPP) technique. We first demonstrate that the pseudorange measurement noise leads to the boundary discontinuity by simulation. We also find that the boundary discontinuity is reduced by 10% - 30% when executing PPP with the input of the IGS 30-sec clock product, instead of the IGS 5-min clock product, by analyzing the real Receiver Independent Exchange Format (RINEX) data. The average of several GPS receivers at the same station can also reduce the impact of pseudorange measurement noise on the boundary discontinuity. The improvement is typically 15% - 20%. Besides, a bad data point in the RINEX file can affect not only the time at that specific epoch, but also the whole time at all epochs and thus the boundary discontinuity, especially when the bad point happens at the boundary of the data-arc. The RINEX-Shift algorithm is designed to eliminate the boundary discontinuity.

A new program, called "NEW PPP", is then developed based on the above analysis and conclusions. The time comparison between NIST and PTB by NEW PPP matches the Two Way Satellite Time and Frequency Transfer (TWSTFT) result better than the conventional PPP result, in terms of the long-term (e.g., 10 days) tendency. This shows that the result of NEW PPP is closer to the true value, compared to the conventional PPP result. The comparison between two distant fountains shows that we are able to observe the UTC(k) clock behavior for an averaging time of greater than 1 day. This fountain comparison also sets up the upper limit of NEW PPP time transfer noise. It is 3×10^{-16} for an averaging time of 10 days.

I. INTRODUCTION

Global Positioning System (GPS) carrier-phase (CP) time transfer is currently a widely accepted method for high precision time transfer [1, 2]. The method provides lower short-term noise than other time transfer methods, such as Two Way Satellite Time and Frequency Transfer (TWSTFT) and Common View (CV) Time Transfer [3].

However, independent daily CP time transfer solutions frequently show day boundary discontinuities of up to 1 ns due to the inconsistency of the phase ambiguity between two independent days [4]. This makes CP time transfer not very useful for the comparison of primary

Proceedings of the 2013 Precise Time and Time Interval Systems and Applications Meeting,
ION PTTI 2013, Bellevue, Washington, December 2-5, 2013

292

frequency standards and similar high accuracy and high precision applications.

The GPS observation equations for pseudorange and CP measurements have the following form, respectively [4]:

$$P_i^j = \left| \vec{x}^j - \vec{x}_i \right| + \Delta_{tropo} + \Delta_{ion} + c\Delta t_i - c\Delta t^j + \Delta MP_i^j + \varepsilon, \tag{1}$$

$$L_i^j = \left| \vec{x}^j - \vec{x}_i \right| + \Delta_{tropo} - \Delta_{ion} + c\Delta t_i - c\Delta t^j + \Delta MP_i^j (carrier) + \varepsilon (carrier) + \lambda N_i^j, \tag{2}$$

where Δt_i is the clock bias of station i, Δt^j is the clock bias of satellite j; Δ_{tropo} and Δ_{ion} are the tropospheric delay and ionospheric delay, respectively; ΔMP_i^j is the multipath correction; ε is the noise term; N_i^j is the phase ambiguity. The multipath and noise terms are different for pseudorange and CP measurements.

Pseudorange measurement is much noisier than CP measurement. It provides accurate but not very precise timing information, while CP measurement provides precise but less accurate timing information due to the uncertainty of the phase ambiguity N_i^j. Pseudorange measurements are used to help fix the phase ambiguity so that we have both accurate and precise time. Many researchers believe that the physical noise in pseudorange measurements can lead to an incorrect phase ambiguity, which can finally lead to a boundary discontinuity [4, 5, 6]. Some researchers also show that the algorithm of fixing the phase ambiguity plays an important role in the boundary discontinuity [4].

In this paper, we focus on the improvement over the conventional PPP method. We begin with details of PPP settings. Then we demonstrate that the pseudorange measurement noise leads to CP time transfer boundary discontinuity by simulation. In Section IV, we study some feasible methods of reducing the boundary discontinuity. In Section V, we propose a new algorithm, called "RINEX-Shift Algorithm", to eliminate the boundary discontinuity. In Section VI, a "NEW PPP" program is developed based on Section IV and Section V. Its performance is evaluated and compared with other time transfer methods. The comparison among TWSTFT, conventional PPP, and NEW PPP shows that NEW PPP gives the best time transfer result. Section VII compares two distant fountains and two distant UTC(k)s by TWSTFT, conventional PPP and NEW PPP.

II. GPS DATA PROCESSING

The NRCan PPP software [7] is run for several GPS receivers in this paper. The default settings are as follows: "USER DYNAMICS" is set to "STATIC" because all receivers used in this paper are in static mode; we use International GNSS Service (IGS) 5-min final products (SP3 and CLK) and Receiver Independent Exchange Format (RINEX) data as the input files for NRCan PPP; the software solves for both the station position and the clock bias; the cutoff elevation is set to 10 degrees. We extract the backward data to get the clock bias because a calculation in this direction provides a better tropospheric delay estimate and the solutions converge better in backward mode [7]. The RINEX-Shift algorithm (Section V) and the NEW PPP program (Section VI & VII) use the same PPP settings as above.

We use the "Overlapping Method" to extract the boundary discontinuity [4]. The Overlapping Method runs PPP first for two consecutive days independently, then runs PPP for the combined two days, and then extracts the difference between the first day and the combined two days $\Delta_{1 \to X}$ and the difference between the combined two days and the second day $\Delta_{X \to 2}$. Then $\Delta_{1 \to 2} = \Delta_{1 \to X} + \Delta_{X \to 2}$ gives the boundary discontinuity between the two days (Figure 1).
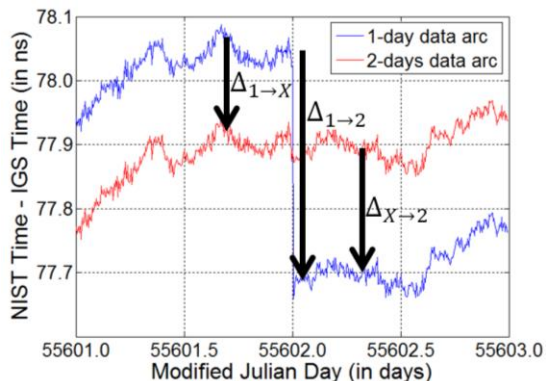

Figure 1. Algorithm of Overlapping Method. $\Delta_{1 \to X}$ is the average time difference between the first day and the combined two days from 15:00 to 21:00. $\Delta_{X \to 2}$ is the average time difference between the second day and the combined two days from 3:00 to 9:00. $\Delta_{1 \to 2} = \Delta_{1 \to X} + \Delta_{X \to 2}$, where $\Delta_{1 \to 2}$ is the jump value estimated by the Overlapping Method [4].

III. MEASUREMENT NOISE AND BOUNDARY DISCONTINUITY

In 2006, two receivers (*NISA* (Ashtech Z12T) and *NISV* (Novatel T-Sync receiver with an OEM4 board)) at NIST were connected to the same antenna [8]. We process the RINEX data on Modified Julian Day (MJD) 53737 and get the measurement difference (Figure 2 and Figure 3) between the two receivers. The measurement difference shows the receiver noise and the cable noise. We can see that the pseudorange measurement has greater noise at a low satellite elevation (Figure 2). Since the two receivers are connected to a common antenna, the tropospheric

Proceedings of the 2013 Precise Time and Time Interval Systems and Applications Meeting,
ION PTTI 2013, Bellevue, Washington, December 2-5, 2013

293

noise, the ionospheric noise and the multipath noise, etc are already cancelled by the measurement differencing. So the greater noise at low satellite elevation in Figure 2 can only come from the receiver performance, e.g., the tracking loop performance for weak signals. As shown in Figure 2, the standard deviation (STD) of the PRN04 C1 pseudorange measurement difference is 0.53 m. The STD of L1 phase measurement difference is 0.012 cycle (Figure 3). If we assume that the two receivers are of the same or similar performance, we get that the pseudorange noise due to receiver and cable is $0.53/\sqrt{2} = 0.37$ m, and that the phase noise due to receiver and cable is $0.012/\sqrt{2} = 0.0085$ cycle. The total measurement noise should be greater than the above result, because satellite orbit, the satellite clock, ionosphere, troposphere and antenna all introduce noise to the measurement. Since the noisy pseudorange (> 0.37 m) is used to solve for the phase ambiguity, the pseudorange noise could have a big impact on the phase ambiguity and boundary discontinuity.
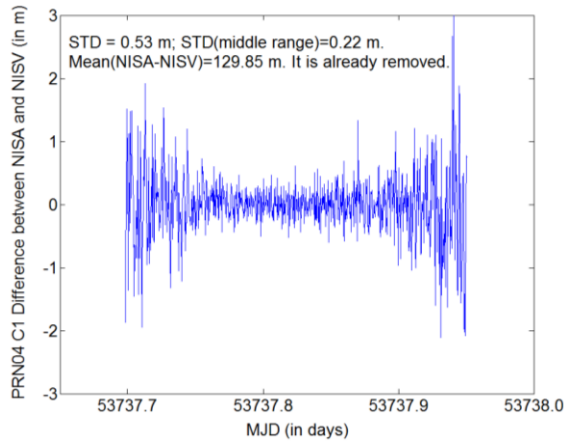

Figure 2. C1 pseudorange measurement difference between *NISA* and *NISV* for PRN04 on MJD 53737. The STD of C1 difference is 0.53 m. If we neglect the low elevation part of C1 measurement, the STD becomes around 0.22 m.
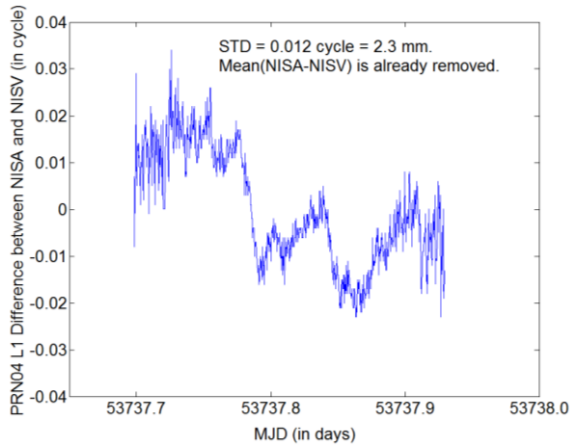

Figure 3. L1 phase measurement difference between *NISA* and *NISV* for PRN04 on MJD 53737. The STD of L1 phase difference is 0.012 cycle, which corresponds to 2.3 mm.

Next, let's simulate the impact of measurement noise on the boundary discontinuity. There are basically two methods to do the simulation. One method is to generate ideal noise-free RINEX data. Then we add noise to the RINEX data and see the change in the boundary discontinuity. The difficulty in this method comes from the generation of noise-free RINEX data. Although there are some software packages available in the world, we do not know the details, e.g., whether it includes the ionospheric and the tropospheric delays. Besides, we may also need to revise PPP in order to remove some correction terms in PPP. The other method is to add white noise to the original measured RINEX data and study the change in boundary discontinuity. This method is easier to implement. Besides, it can reveal the relation between measurement noise and boundary discontinuity quite effectively.

Here, we choose the second method to do the simulation. First, we keep the phase noise at the noise level of 0.01 cycle and increase the pseudorange noise from 0.0 m to 0.5 m (Figure 4). 1000 trials are done for each pseudorange noise level in order to get a reliable statistical distribution. From Figure 4, we can see that the STD of the clock offset at epoch 0 (that is, the very beginning epoch of the day) increases almost linearly as the pseudorange noise increases. For the pseudorange noise of 0.3 m and the phase noise of 0.01 cycle, which is a very common receiver performance as indicated in Figure 2 and Figure 3, the STD is 85 ps, which corresponds to the STD of the boundary discontinuity of 85 ps $\times \sqrt{2}$ = 120 ps. This value matches the statistical result of the boundary discontinuity in Section IV of [4] quite well. From Figure 5, we can see that the STD of the clock offset at epoch 0 changes little for the phase noise in the range of 0.00 − 0.02 cycle. For most geodetic receivers, the phase noise is around 0.01 cycle or even less. That means, the phase noise has little impact on boundary discontinuity. Figure 6 studies the relation between the short-term (300 sec) stability of CP time transfer and the measurement noise. The time deviation (TDEV) at the averaging time of 300 sec is used to characterize the short-term stability. The six curves are very close to each other, which indicates that the pseudorange noise has little impact on the short-term stability of CP time transfer. TDEV (300 sec) increases from 8 ps to around 50 ps as the phase noise increases from 0 cycle to 0.05 cycle. This shows that the phase measurement plays an important role in the short-term CP time transfer.

The above analysis indicates that the pseudorange noise is very critical to the boundary discontinuity. If we can estimate the terms on the right side of eq. (1) better, we can reduce ε and thus reduce the boundary discontinuity. Another way is to have more receivers so that we have more GPS observation equations. In this way, the boundary discontinuity is averaged down and the local time can be better estimated. We will explore these conjectures in Section IV.

Proceedings of the 2013 Precise Time and Time Interval Systems and Applications Meeting,
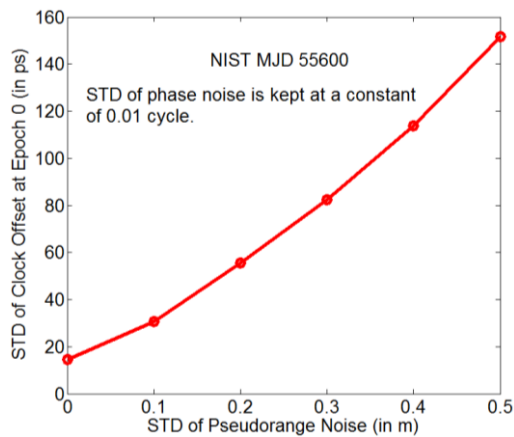**ION PTTI 2013, Bellevue, Washington, December 2-5, 2013**

294

Figure 4. Relation between the clock offset at epoch 0 and the pseudorange noise (simulation result). The phase noise is kept at the STD of 0.01 cycle.
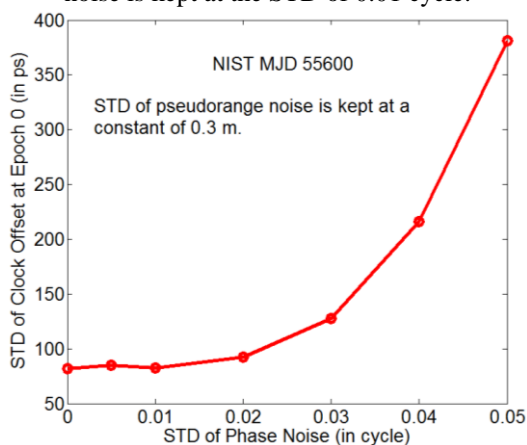

Figure 5. Relation between the clock offset at epoch 0 and the phase noise (simulation result). The pseudorange noise is kept at the STD of 0.3 m.
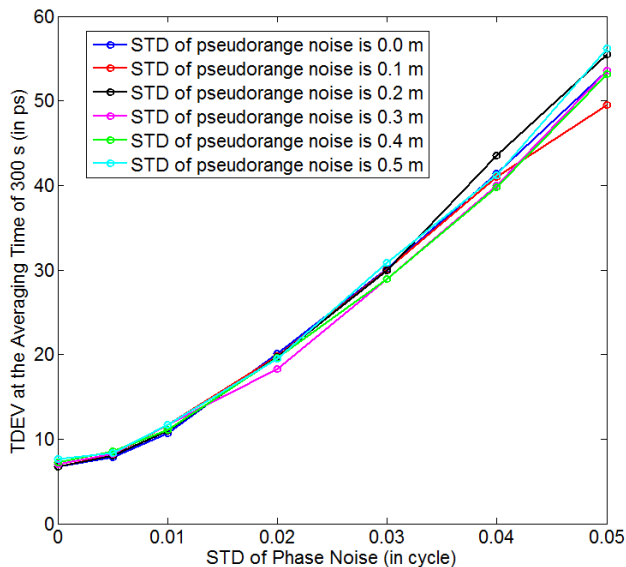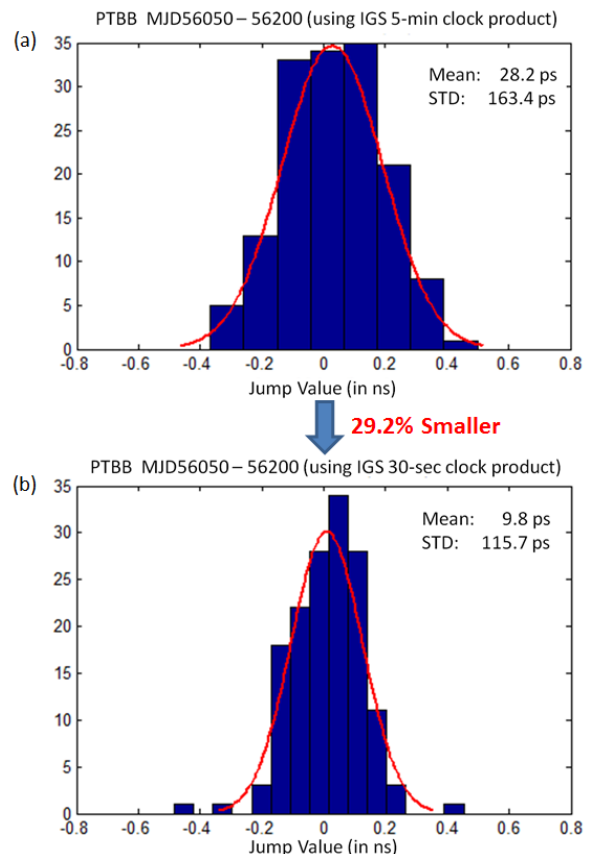

Figure 6. TDEV at 300 sec for different pseudorange noise and phase noise levels (simulation result).

IV. METHODS OF REDUCING BOUNDARY DISCONTINUITY

1. IGS Clock Product and Boundary Discontinuity

According to Section III, one way of reducing the boundary discontinuity is to estimate the terms on the right side of equation (1) better. IGS provides the IGS 30-sec clock product which has more information about the satellite clocks than the IGS 5-min clock product. So using the IGS 30-sec clock product as the input of PPP could potentially reduce the boundary discontinuity.

Figure 7 confirms this assumption. We run PPP for *PTBB* (a GPS receiver in PTB, Germany) from MJD 56050 to MJD 56200 with the IGS 5-min clock product as the input (Figure 7(a)). The STD of the boundary discontinuity jump values is 163.4 ps. Then we run PPP for *PTBB* with the IGS 30-sec clock product as the input (Figure 7(b)). The STD of jump values becomes 115.7 ps. The improvement over the boundary discontinuity by using the IGS-30sec clock product is as big as 29.2% for *PTBB*. Similarly, for *PTBG* (also in PTB, Germany), the improvement is 22.8% (Figure 7(c)-(d)). Besides, the mean value of the boundary discontinuity also becomes closer to 0 ps for both *PTBB* and *PTBG*.

Proceedings of the 2013 Precise Time and Time Interval Systems and Applications Meeting,
ION PTTI 2013, Bellevue, Washington, December 2-5, 2013
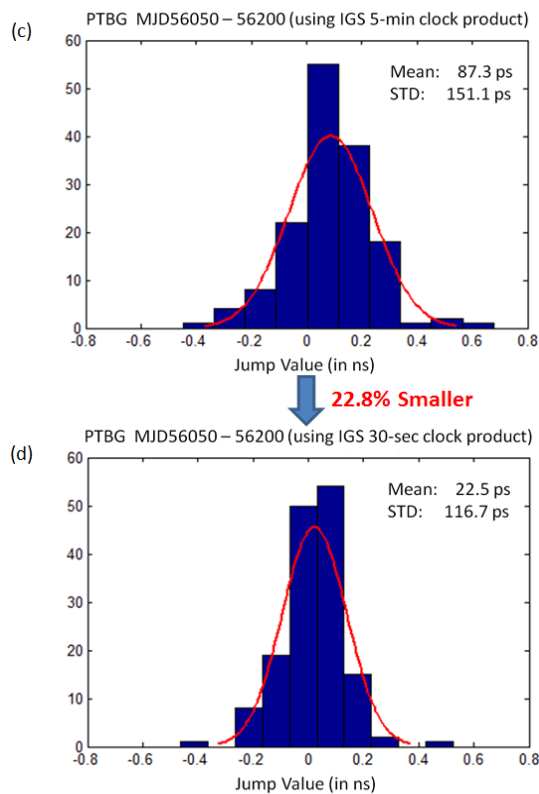
295

Figure 7. Boundary discontinuity by using the IGS 5-min clock product vs boundary discontinuity by using the IGS 30-sec clock product, for *PTBB* and *PTBG* from MJD 56050 to MJD 56200.

Figure 8 is the time difference between *PTBB* and *PTBG*. In principle, the difference should be a constant because they have the same reference clock [9]. In practice, the cable extension and the receiver aging, etc make it not exactly a constant. The blue curve is the time difference between the two receivers by using the IGS 5-min clock product. The red curve is the time difference using the IGS 30-sec clock product. The blue curve is obviously noisier than the red curve. This indicates that the time transfer result using the IGS 30-sec clock product is closer to the true values than that using the IGS 5-min clock product.

Figure 9 shows the improvement over the boundary discontinuity using the IGS-30sec clock product at several timing laboratories in the world. The improvement is typically 10% - 30%.

2. Average of Receivers and Boundary Discontinuity

According to Section III, another way to reduce the boundary discontinuity is to use more GPS receivers to transfer time so that the pseudorange noise can be averaged down. For two receivers, we have eq. (1) and eq. (2) for each receiver. The two receivers are typically connected to two different antennas, instead of to a common antenna. This makes the direct averaging over the pseudor-

ange and the phase measurements of the two receivers not feasible, because they are at different physical locations. A better and easier way is to estimate the time for each receiver by PPP first and then do averaging over the time results. In this way, all receivers at the same station, even though they are not connected to a common antenna, can be used.
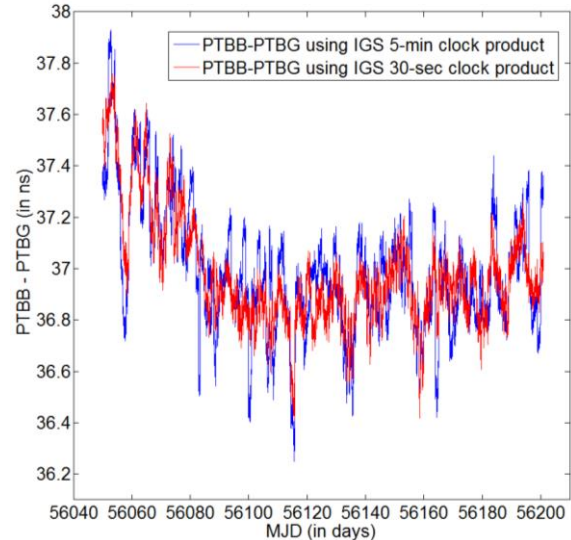

Figure 8. Time difference between *PTBB* and *PTBG* by using the IGS 5-min clock product (blue curve) and by using the IGS 30-sec clock product (red curve).
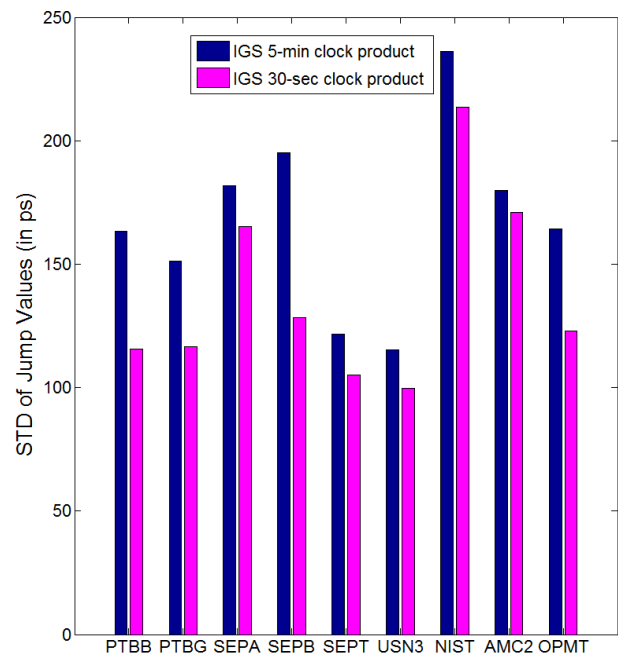

Figure 9. Boundary discontinuity by using the IGS 5-min clock product vs boundary discontinuity by using the IGS 30-sec clock product, for several GPS receivers in the world (*PTBB* 56050-56200, *PTBG* 56050-56200, *SEPA* 55927-56077, *SEPB* 55927-56077, *SEPT* 55927-56077, *USN3* 56050-56200, *NIST* 55600-55750, *AMC2* 56050-56200 and *OPMT* 56050-56200).

Proceedings of the 2013 Precise Time and Time Interval Systems and Applications Meeting,
ION PTTI 2013, Bellevue, Washington, December 2-5, 2013

296

For *NISA* at NIST, the STD of the boundary discontinuity jump values is 167.2 ps for MJD 56230 – 56380. For *NISX* at NIST, the STD is 215.0 ps for the same period. If we do averaging over the two receivers, the STD becomes 124.0 ps, which indicates an improvement of 25.8%. We also do averaging for *SEPA* and *SEPB* at NICT (Japan) for MJD 55927 – 56077, and *PTBB* and *PTBG* at PTB for MJD 56050 – 56200. The improvements by averaging two receivers at the same station are 13.7% and 15.9%, respectively (Figure 10).
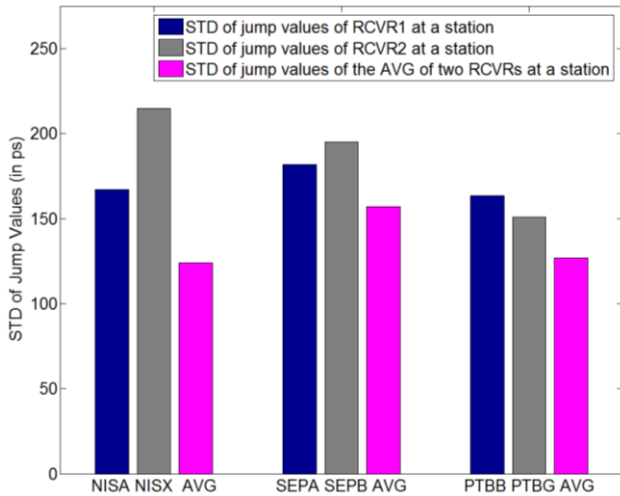

Figure 10. Average of receivers and boundary discontinuity for NIST (*NISA* and *NISX*), NICT (*SEPA* and *SEPB*) and PTB (*PTBB* and *PTBG*). The magenta bar is the average of two receivers at a station.

The average of receivers also helps reduce the short-term (< 30 min) noise by 10% - 20% (Figure 11). On the other hand, this also indicates that the conventional CP time transfer cannot observe the short-term (<30 min) clock noise very well because the actual clock noise cannot be averaged down by using two GPS receivers.
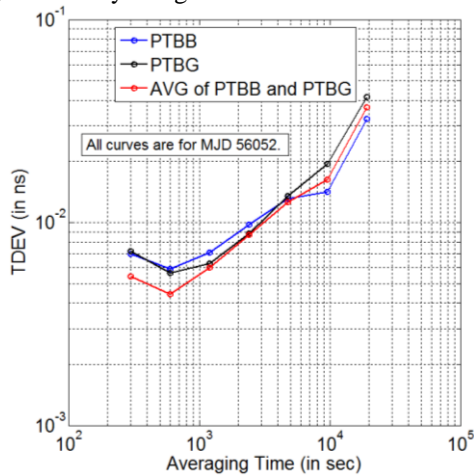

Figure 11. Improvement of the average of receivers on the short-term time transfer frequency stability. For the averaging time of 5 min and 10 min, the average of receivers gives an improvement of 10%-20%.

3. Bad Points and Boundary Discontinuity

We find that a bad data point in the RINEX file can affect not only the time at that specific epoch, but also the whole time at all epochs and thus the boundary discontinuity, especially when the bad point happens at the beginning or at the end of the data-arc. For example, we run PPP for *NIST* with the input of the RINEX data-arc from 19:40:00 to 19:39:30 of the next day (e.g., from 19:40:00 of MJD 55647 to 19:39:30 of MJD 55648). This is shown by the blue curve in Figure 12 (blue, red and black curves are very close except for the second data-arc in Figure 12.). We can see that the boundary discontinuity is obviously below 500 ps. However, if we shift the RINEX data-arc by 5 min (that is, we run PPP for the data-arc from 19:45:00 to 19:44:30 of the next day (red curve in Figure 12)), the boundary discontinuity is now greater than 3 ns. This huge boundary discontinuity comes from the bad point happening at 19:40:00 of MJD 55649. If we remove the two bad PRNs (PRN14 and PRN31) measurements at this epoch, then the huge boundary discontinuity disappears (magenta curve, which is very close to the green curve and the black curve). Black curve shows the case of data-arc of 19:50:00 to 19:49:30 of the next day. The boundary discontinuity of the black curve is again smaller than 500 ps. This example shows that if a bad data point happens at the end of the data-arc, we could have a huge boundary discontinuity.
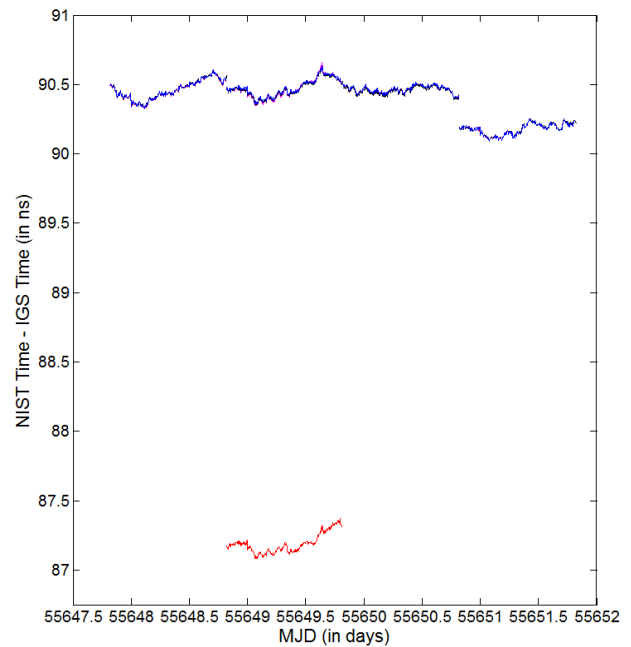

Figure 12. Illustration of the impact of a bad data point on the boundary discontinuity. The blue curve is the result for the data-arc of 19:40:00 to 19:39:30 of the next day. The red curve is the result for the data-arc of 19:45:00 to 19:44:30 of the next day. The magenta curve is the corrected result of the red curve on the second data-arc after the bad data are removed. The black curve is the result for the data-arc of 19:50:00 to 19:49:30 of the next day.

Proceedings of the 2013 Precise Time and Time Interval Systems and Applications Meeting,
ION PTTI 2013, Bellevue, Washington, December 2-5, 2013

297

Bad points can not only seriously affect the boundary discontinuity as mentioned above, but also damage the whole time transfer result (such as the slope) of a single data-arc. Figure 13 shows this. We have already detected that there are a few bad points between 15:00:00 and 16:00:00 of MJD 55647 for *USN3* (at USNO, USA). This period (MJD 55647.625 – 55647.667) is marked by the big black rectangle in Figure 13. At the time around MJD 55646.5, all curves are approximately parallel. That indicates the slope is almost the same no matter how we shift the RINEX data, which is what we expect. The difference between two adjacent curves is around 0.2 ns. The slight difference from 0.2 ns comes from different boundary discontinuities due to shifted data-arcs. The same situation occurs at around MJD 55648.5. However, the slopes of all curves are not the same around MJD 55647.5 due to the bad points happening from 15:00:00 to 16:00:00 on this day. For example, at MJD 55647.60, the bottom black curve reads 7.685 ns. The bottom red curve almost reads the same value as the bottom black curve. At MJD 55647.75, the bottom red curve reads 7.817 ns. However, the bottom black curve reads 7.607 ns. The slope difference between the two curves during MJD 55647.60 – 55647.75 is as big as 1.4 ns/day. Remember that we use exactly the same RINEX data and run PPP with exactly the same settings. The only difference is that we shift the RINEX data by a few hours. In principle, the slope difference of two curves should be very close to 0. Because of the existence of bad points, we have totally different time transfer results, which makes it hard to tell which one is correct or both of them are wrong. This example demonstrates how seriously a few bad points can damage the whole time transfer result of a single data-arc.
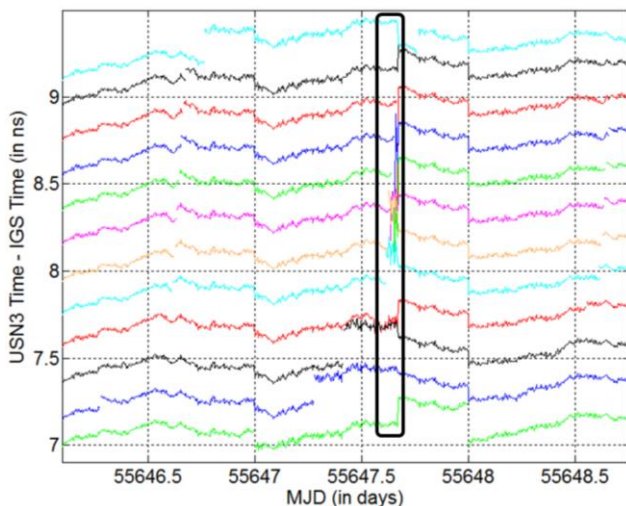

Figure 13. Illustration of how bad points damage the time transfer result of the same data-arc. The curves are shifted along the y-axis by multiple of 0.2 ns for better comparison. Each curves starts at different start points (e.g., the magenta curve starts at 15:15:00; the bottom green curve starts at 00:00:00).

From Figure 13, we also know that bad points are easier to be detected at the boundary of a data-arc. The top cyan curve, bottom black curve, bottom blue curve and bottom green curve are the CP results when bad points are in the middle range of the data-arc. The bottom blue curve is very smooth, which hides the bad points. The top cyan, bottom black and bottom green only show that there is a single bad point at 16:00:00. If we shift the data-arc so that the bad points are around the boundary (all other curves), we can notice that there are many bad points between 15:00:00 and 16:00:00.

V. RINEX-SHIFT ALGORITHM

The RINEX-Shift algorithm is designed to eliminate boundary discontinuity. Figure 14 shows how the algorithm works. The conventional PPP runs first forward (from the beginning of the data-arc to the end of the data-arc) and then backward (from the end of the data-arc to the beginning of the data-arc) in order to converge the solutions [7]. The backward results (a point every 5 min) form the final PPP output. As shown in Figure 14(a), the blue dots and the red dot are the backward results of PPP. Since the phase ambiguity is almost always away from the true value due to the pseudorange noise, the solution of one data-arc almost always has a gap from the solution of the next data-arc. This gap is the boundary discontinuity. Since the pseudorange noise is impossible to remove, even though it can be reduced as stated in Section IV, a good way to "eliminate" the boundary discontinuity is to make the length of data-arc to be 5 min so that every point has its own estimation of phase ambiguity. Now the boundary discontinuity is actually transformed from a long data-arc (>= 1 day) to a short data-arc (e.g., 5 min). The boundary discontinuity of a short data-arc cannot be noticed because it is combined with the short-term (e.g., 5 min) noise. In this way, we no longer have the boundary discontinuity, and the CP time transfer can be used for a long-term (e.g., 20 days) time comparison without the impact of the boundary discontinuity. Another thing to consider is that using a short data-arc can hardly give a converged estimate of zenith path delay of the troposphere, etc, so that the short-term noise can be very huge because of the big uncertainty in the phase ambiguity. A good way to tackle this issue is to run PPP for a long data-arc and extract the result at the first epoch point of the backward process (the red dot in Figure 14(a)). Then we shift the RINEX data by another time step (e.g., 5 min, or 10 min, or even greater) and executes PPP, and extracts the result at the new first epoch again (Figure 14(b)). So on and so forth (Figure 14(c)-(d)). The results at all first epochs (the red dots in Figure 14(a)-(d)) form the final result. In this way, we can not only eliminate the boundary discontinuity but also have small short-term noise. We call this algorithm the "RINEX-Shift Algorithm". Because the RINEX-Shift algorithm makes each epoch at the boundary of the data-arc with a specific shift and bad points are more likely to be

Proceedings of the 2013 Precise Time and Time Interval Systems and Applications Meeting,
ION PTTI 2013, Bellevue, Washington, December 2-5, 2013

298

detected at the boundary as stated in Part 3 of Section IV, this algorithm can also be used to detect bad points.
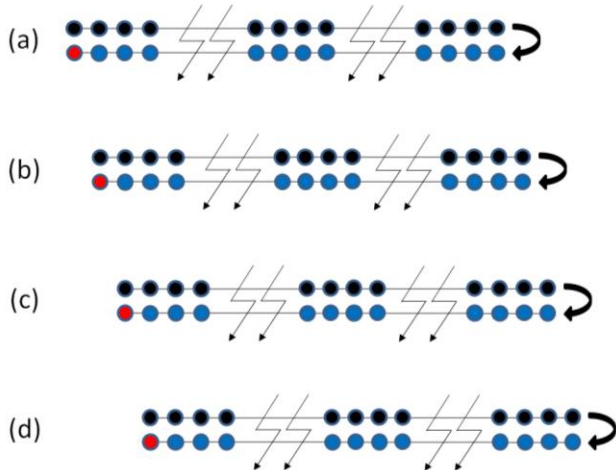

Figure 14. Illustration of the RINEX-Shift algorithm.

VI. NEW PPP

Based on the analysis in Section IV and Section V, we develop a program called "NEW PPP". This program runs PPP by the RINEX-Shift algorithm with the IGS 30-sec clock products as the input, for several receivers at the same station. Besides, it also removes the bad points with 4σ confidence level. The final time comparison result is the average of the time comparison results of the several receivers.

For the purpose of testing this program, we choose two GPS receivers at NIST (*NIST* and *NIS2*) and two GPS receivers at PTB (*PTBB* and *PTBG*). We set the data-arc of the RINEX-Shift algorithm to 10 days and the time step to 10 min. Then we run the NEW PPP and get the time difference between the NIST time (UTC(NIST)) and the PTB time (UTC(PTB)) during MJD 56389 – 56409 (red curve in Figure 15). The blue curve is the result of the conventional PPP with a 1-day data-arc. The modified total deviation (MTD) is used to characterize the frequency stability (Figure 16). The NEW PPP reduces the time-transfer noise significantly, especially at the range of 4 hours to 4 days. The MTD of the NEW PPP result (red curve in Figure 16) becomes flat for an averaging time of greater than 1 day, which indicates that we have already seen the clock noise after 1 day. We will discuss this further in Section VII. Figure 17 is the frequency stability test of the NEW PPP for another time range (using *NIST*, *NISX*, *PTBB* and *PTBG*, because *NIS2* has some weird behaviors at this time range). It is provided for redundancy so that we have more information on the NEW PPP performance.

As stated in [6], the smoothest time-transfer solution is not necessarily the most accurate solution. The above analysis only shows that the NEW PPP does provide a smoother solution than the conventional PPP with a 1-day data-arc. Next, we need to test the accuracy of the NEW PPP. This

is done by comparing the NEW PPP with the conventional PPP results and TWSTFT (Figure 18).
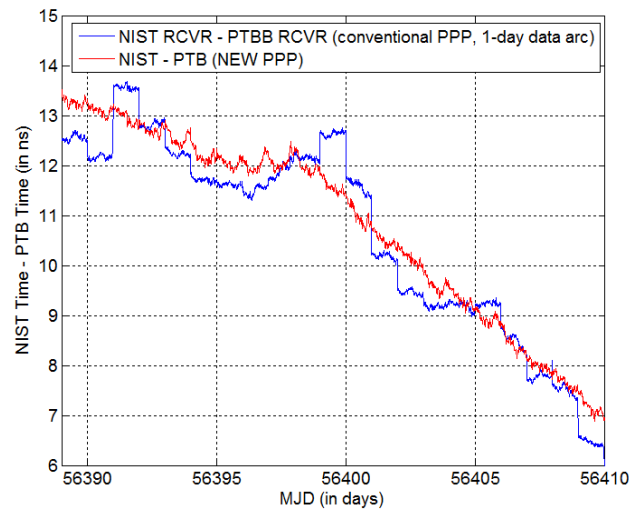

Figure 15. Time comparison between UTC(NIST) and UTC(PTB) during MJD 56389 – 56409 by the conventional PPP and the NEW PPP. The curves are shifted by some constants for better comparison.
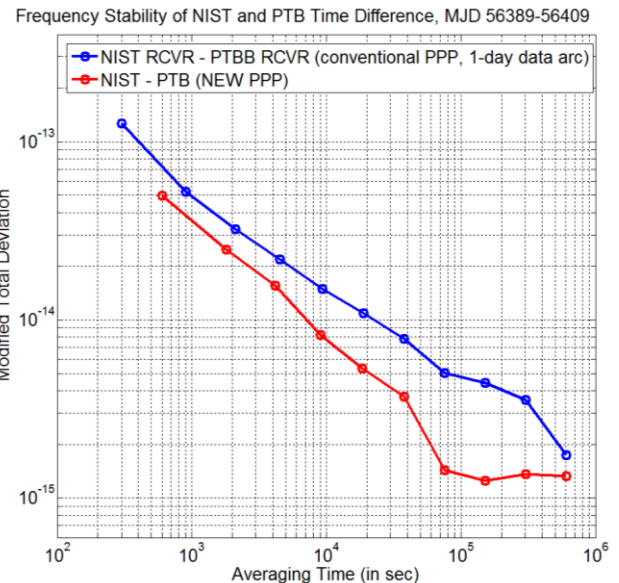

Figure 16. MTD of time difference between UTC(NIST) and UTC(PTB) for MJD 56389 – MJD 56409, by using the conventional PPP with a 1-day data-arc (blue curve) and by using the NEW PPP (red curve).

Proceedings of the 2013 Precise Time and Time Interval Systems and Applications Meeting,
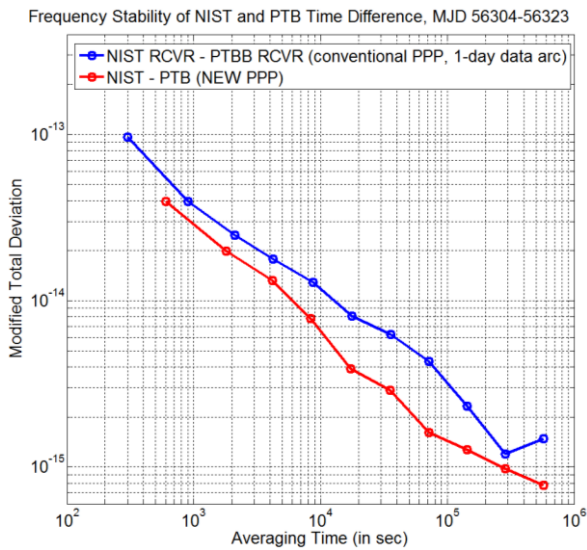**ION PTTI 2013, Bellevue, Washington, December 2-5, 2013**

299

Figure 17. MTD of time difference between UTC(NIST) and UTC(PTB) for MJD 56304 – MJD 56323 (some bad RINEX data on MJD 56308 and 56316 are removed), by using the conventional PPP with a 1-day data-arc (blue curve) and by using the NEW PPP (red curve).

We can see that TWSTFT (blue curve in Figure 18) has a diurnal oscillation which makes it not good for the short-term time transfer. The conventional PPP with a 1-day data-arc typically has a boundary discontinuity each day, which degrades the long-term time transfer result. Besides, the slope of each day also does not match the tendency of TWSTFT well. For example, the black curve goes up on MJD 56378, while the blue curve goes down. For another example, the black curve is flat on MJD 56401, while the blue curve tends to go down. This inconsistency between TWSTFT and the conventional PPP indicates that the conventional PPP could have a wrong slope and thus an incorrect time comparison result. The conventional PPP with a 10-day data-arc (magenta curve in Figure 18) and the conventional PPP with a 30-day data-arc (orange curve in Figure 18) also do not match TWSTFT very well, though they are better than the conventional PPP with a 1-day data-arc. We can see that the magenta curve drifts away from the blue curve. Then there is a boundary discontinuity which makes it match the blue curve again (e.g., the boundary at MJD 56385.0, 56405.0, 56425.0, and
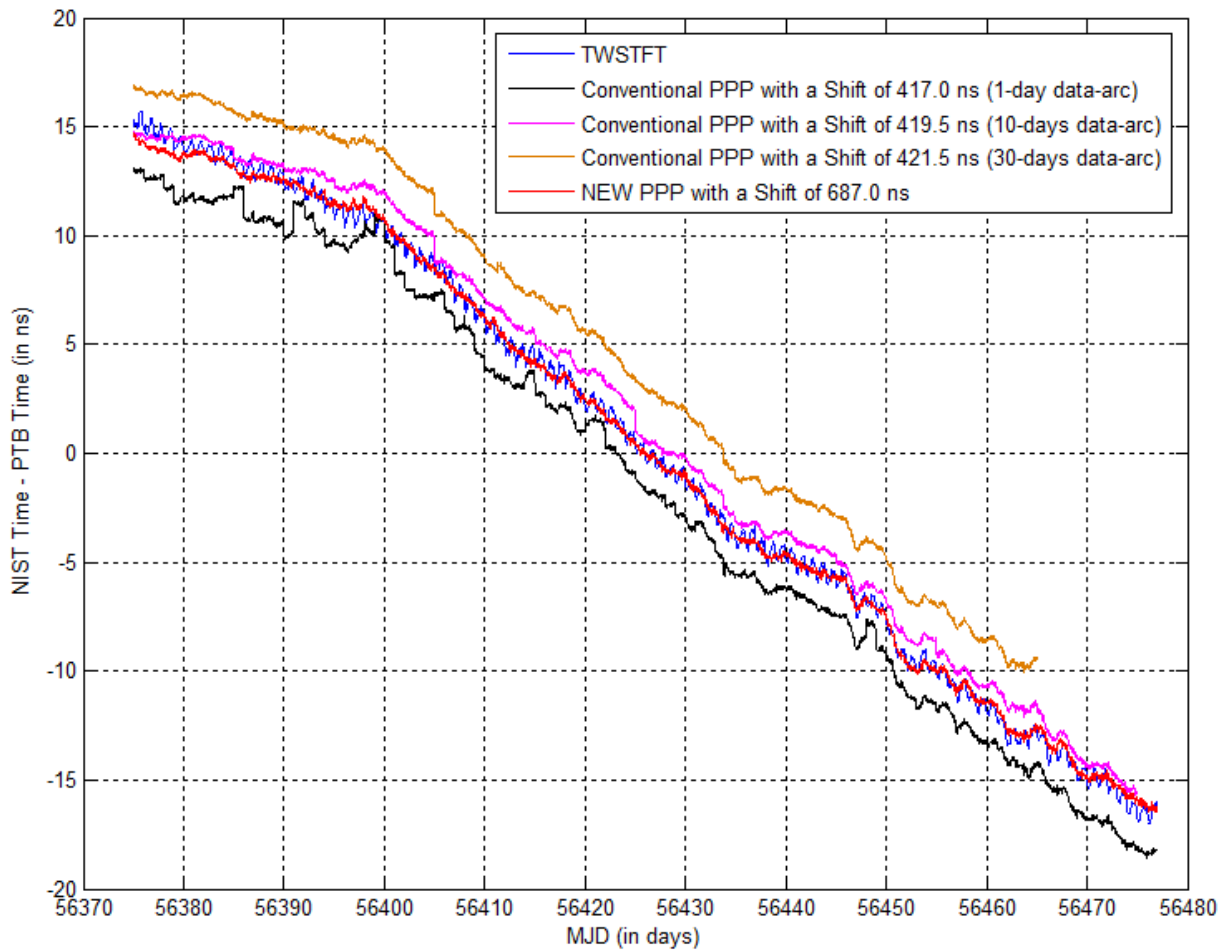

Figure 18. Time difference between UTC(NIST) and UTC(PTB) for MJD 56375 – 56476 by using TWSTFT (blue curve), conventional PPP with a 1-day data-arc (black curve), conventional PPP with a 10-day data-arc (magenta curve), conventional PPP with a 30-day data-arc (orange curve) and NEW PPP (red curve).

Proceedings of the 2013 Precise Time and Time Interval Systems and Applications Meeting,
ION PTTI 2013, Bellevue, Washington, December 2-5, 2013

300

56455.0, etc). So the slope and the boundary discontinuity compensate each other. Since the boundary discontinuity should not appear in nature, we can say that the conventional PPP result has an incorrect slope. Some people propose that we can use a longer data-arc (e.g., 35 days or 40 days) in order to avoid the appearance of the boundary discontinuity in the time range we are interested [10]. This method can still hardly avoid the incorrect slope. So the time comparison by using the conventional PPP with a super long data-arc could still introduce some man-made error. The "NEW PPP" result (red curve in Figure 18) matches TWSTFT very well. The boundary discontinuity disappears and the slope also matches the tendency of TWSTFT quite well. In order to characterize how well all PPP curves match TWSTFT mathematically, we study the MTD of the difference between TWSTFT and each PPP (Figure 19). We can see that "TWSTFT – NEWPPP" (red curve in Figure 19) has the smallest fractional frequency in a long term (> 1 day), which means that the NEW PPP matches TWSTFT best. This confirms our observation in Figure 18.

Comparison between two receivers at the same station is a good test for a time transfer method because the reference clock noise is cancelled out and only the time transfer noise is left. Figure 20 shows the time difference between the "*NIST*" receiver and the "*NIS2*" receiver at NIST by using different time transfer methods. The conventional PPP results (blue curve, black curve and orange curve) are quite artificial. The time difference between two common-reference-clock receivers is not continuous. Besides, the slopes of black curve and orange curve are not zero. The slope and the boundary discontinuity compensate each other in order to keep the curve flat in a long term. In contrast, the NEW PPP (red curve) seems closer to the true value. The curve is continuous. The oscillation in the red curve could come from the cable expansion, the multipath, and some receiver and antenna behaviors.

Figure 20. Time difference between *NIST* and *NIS2* for MJD 56375 – MJD 56476, by using different PPP time transfer methods (conventional PPP with a 1-day data-arc (blue curve), conventional PPP with a 10-day data-arc (black curve), conventional PPP with a 30-day data-arc (orange curve), and NEW PPP (red curve)).

VII. FOUNTAIN COMPARISON AND UTC(K) COMPARISON BY NEW PPP

The purpose of time transfer is to compare two distant clocks. We are always interested in observing the behavior of a remote clock by using a time transfer method [11]. Cesium fountain, as a primary frequency standard, is supposed to be very accurate in a long term (e.g., > 5 days). In contrast, other timing systems (such as H-maser, UTC(k), etc) are more likely to walk away from the right time after a few days. However, the long-distance clock behavior measurement is typically damaged by the time transfer
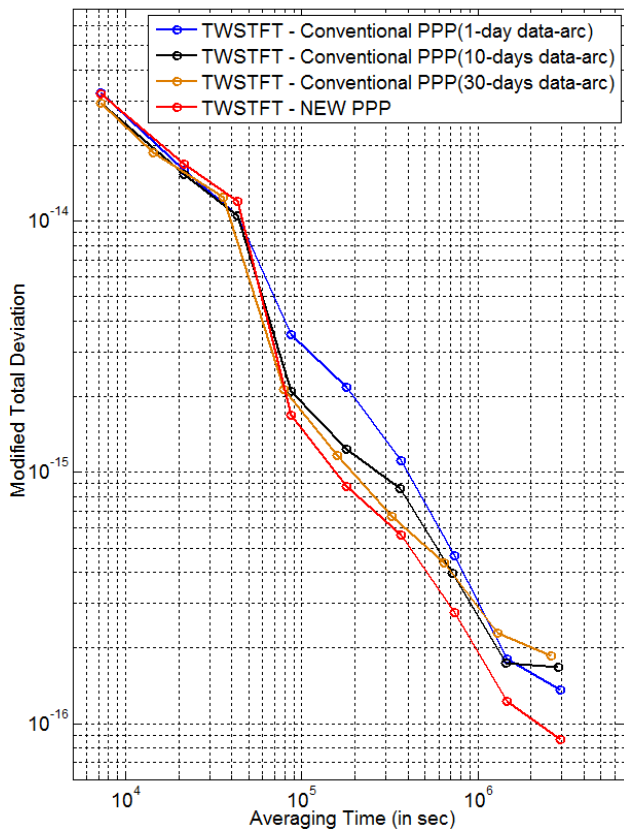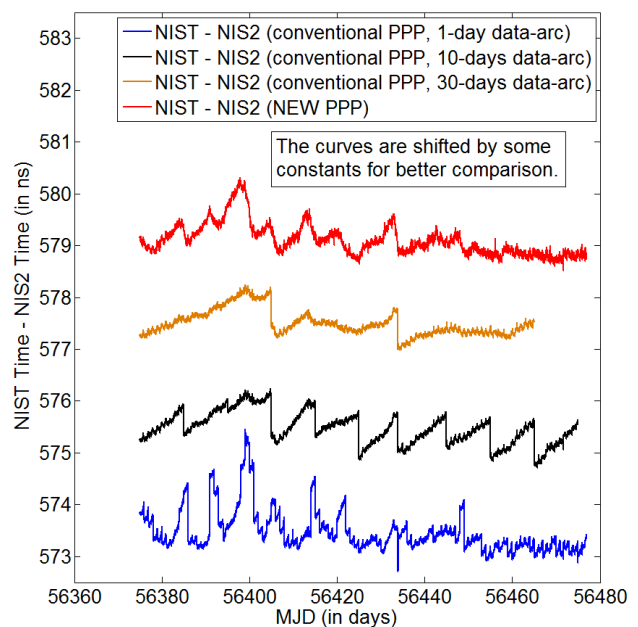

Figure 19. MTD of the double-difference between TWSTFT and different PPP time transfer methods (conventional PPP with a 1-day data-arc (blue curve), conventional PPP with a 10-days data-arc (black curve), conventional PPP with a 30-day data-arc (orange curve), and NEW PPP (red curve)), for MJD 56375 – 56476.

Proceedings of the 2013 Precise Time and Time Interval Systems and Applications Meeting,
ION PTTI 2013, Bellevue, Washington, December 2-5, 2013

301

noise for a short term (< 1 day). The time transfer noise decreases faster than the clock noise as the averaging time increases. So it is possible for us to start to observe the clock behavior after a few days. When comparing two long-distance UTC(k)s, the time difference has both clock noise and time transfer noise. It is hard to distinguish them. Since the Cesium fountain is the primary standard, which is supposed to be very accurate in a long term, the cesium fountain clock noise is small compared to the UTC(k) clock noise after a long time. If the time transfer noise is not the dominant noise, we can see that the "long-distance fountain versus fountain" noise is smaller than the "long-distance UTC(k) versus UTC(k)" noise, which indicates that we observe the UTC(k) clock noise.

We pick up one data point (the beginning of the day) each day because PTB provides fountain data only once per day. So the diurnal effect of TWSTFT is suppressed very well (this explains why TWSTFT is even better than the conventional PPP in Figure 22). The original result after linear fitting is shown in Figure 21. The result of frequency stability analysis is shown in Figure 22. From Figure 21 and Figure 22, we can see that the fountain-vs-fountain noise (see the red solid curve in Figure 21 and Figure 22) is smaller than the UTC(NIST)-vs-UTC(PTB) noise (see the red dot curve in Figure 21 and Figure 22) by using the NEW PPP. That means, we have successfully observed the UTC(k) clock behavior for an averaging time of greater than 1 day. Other time transfer methods provide the similar result, but the stability improvement from UTC(NIST)-vs-UTC(PTB) to fountain-vs-fountain is not as big as the NEW PPP. This indicates that the NEW PPP transfer noise contributes least to the total time comparison noise among the three time transfer methods.

Since the red solid curve in Figure 22, as the total noise of the time comparison, has both the NEW PPP time transfer noise and the fountain clock noise and these two noise sources are independent, we can actually get the upper limit of the NEW PPP time transfer noise. For an averaging time of 10 days, the NEW PPP time transfer noise is less than 3×10^{-16}. The red curve in Figure 19 can also set up the upper limit of NEW PPP time transfer noise (e.g., the NEW PPP time transfer noise is less than 2.2×10^{-16} for an averaging time of 10 days). Because both TWSTFT and PPP need to have signals through the troposphere and ionosphere, they could have some common modes which might make the upper limit lower than what it should be. So conservatively, we choose the red solid curve in Figure 22 as the upper limit of NEW PPP time transfer noise.
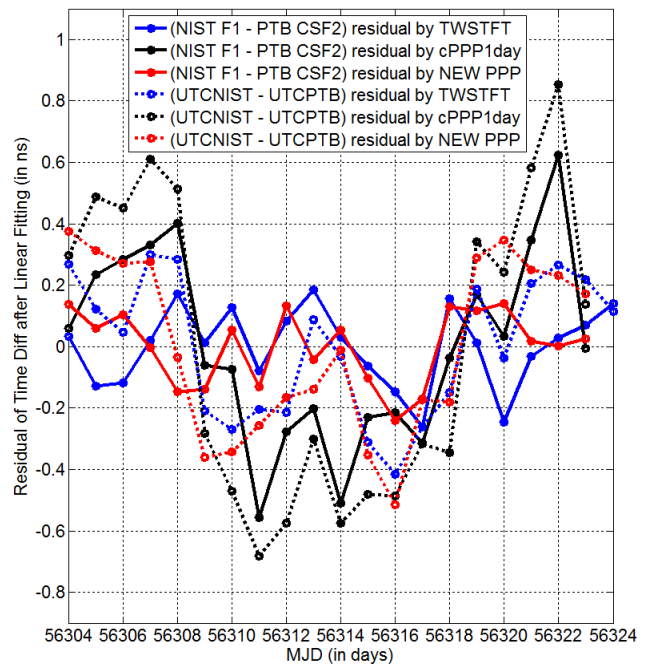

Figure 21. Residuals of the time difference between NIST and PTB after linear fitting. The dotted curves are the time difference between UTC(NIST) and UTC(PTB). The solid curves are the time difference between NIST F1 Fountain and PTB CSF2 Fountain. Blue for TWSTFT, black for the conventional PPP with a 1-day data-arc (cPPP1day, for short), and red for the NEW PPP.
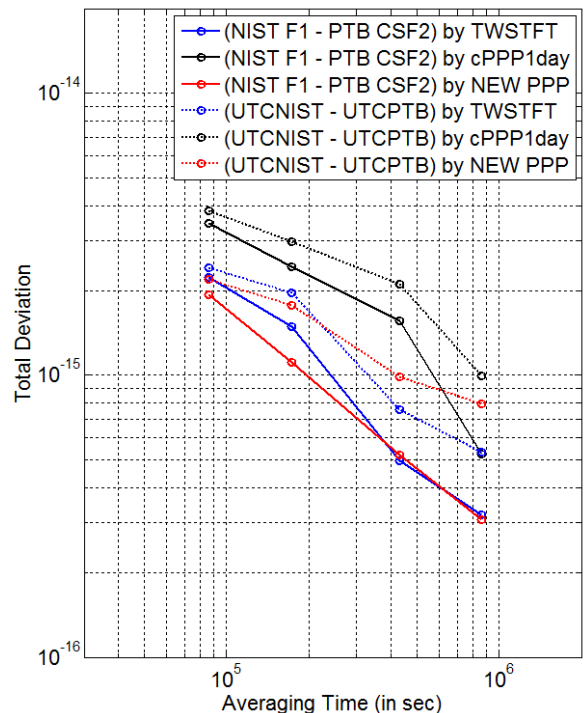

Figure 22. Total deviation of the time difference between NIST and PTB. The curves have the same meaning as Figure 21.

Proceedings of the 2013 Precise Time and Time Interval Systems and Applications Meeting,
ION PTTI 2013, Bellevue, Washington, December 2-5, 2013

302

VIII. CONCLUSIONS

We demonstrate that the pseudorange measurement noise leads to the CP time transfer boundary discontinuity by simulation. We find that the boundary discontinuity is reduced by 10% - 30% when the IGS 5-min clock product is replaced by the IGS 30-sec clock product. The average of several GPS receivers at the same station can also reduce the impact of pseudorange measurement noise on the boundary discontinuity. The improvement is typically 15% - 20%. Besides, it is important to detect the bad data points in order to reduce the boundary discontinuity. The RINEX-Shift algorithm is designed to eliminate the boundary discontinuity and detect bad points.

NEW PPP is developed based on the above conclusions. The NEW PPP result matches the TWSTFT result better than the conventional PPP result, for a long term. This indicates that the NEW PPP approaches to the true value more closely, compared with the conventional PPP result. The comparison between NIST Cs fountain and PTB Cs fountain shows that we are able to observe the UTC(k) clock behavior for an averaging time of greater than 1 day. This fountain comparison also sets up the upper limit of the NEW PPP time transfer noise. For an averaging time of 10 days, the upper limit of the NEW PPP time transfer noise is 3×10^{-16}.

REFERENCES

[1] K. M. Larson and J. Levine, "Carrier-phase time transfer," IEEE Trans. Ultrason., Ferroelect., Freq. Contr., vol. 46, pp. 1001-1012, 1999.

[2] C. Hackman, J. Levine, T. E. Parker, D. Piester, and J. Becker, "A straightforward frequency-estimation technique for GPS carrier-phase time transfer," IEEE Trans. Ultrason., Ferroelect., Freq. Contr., vol. 53, pp. 1570-1583, 2006.

[3] J. Levine, "A review of time and frequency transfer methods," Metrologia, 45, S162-S174, 2008.

[4] J. Yao and J. Levine, "GPS carrier-phase time transfer boundary discontinuity investigation," Proc. 44th PTTI Meeting, pp. 317-326, 2012.

[5] P. Defraigne and C. Bruyninx, "On the link between GPS pseudorange noise and day-boundary discontinuities in geodetic time transfer solutions," GPS Solutions, vol. 11, pp. 239-249, 2007.

[6] R. Dach, T. Schildknecht, U. Hugentobler, L.-G. Bernier, and G. Dudle, "Continuous geodetic time transfer analysis method," IEEE Trans. Ultrason., Ferroelect., Freq. Contr., vol. 53, no. 7, pp. 1250-1259, 2006.

[7] J. Kouba and P. Heroux, "Precise point positioning using IGS orbit and clock products," GPS Solutions, vol. 5, pp. 12-28, 2001.

[8] M. Hottovy and M. Weiss, "Differential delay between two geodetic GPS receivers for L1 and L2 code and carrier signals," Proc. IEEE IFCS 2008 Conference, pp. 496-500, 2008.

[9] C. Hackman and J. Levine, "New frequency comparisons using GPS carrier-phase time transfer," Proc. IEEE IFCS 2003 Conference, pp. 258-265, 2003.

[10] G. Petit, "The TAIPPP pilot experiment," Proc. EFTF-IFCS 2009 Joint Conference, pp. 116-119, 2009.

[11] A. Bauch, J. Achkar, S. Bize, D. Calonico, R. Dach, R. Hlavac, L. Lorini, T. Parker, G. Petit, D. Piester, K. Szymaniec, and P. Uhrich, "Comparison between frequency standards in Europe and the USA at the 10-15 uncertainty level," Metrologia, 43, pp. 109-120, 2006.

Proceedings of the 2013 Precise Time and Time Interval Systems and Applications Meeting,
ION PTTI 2013, Bellevue, Washington, December 2-5, 2013

303